Giant Magnetic Anisotropy Induced by Ligand *LS* Coupling in Layered Cr Compounds

Dong-Hwan Kim,[1,2] Kyoo Kim,[2] Kyung-Tae Ko,[1,2] JunHo Seo,[1,3] Jun Sung Kim,[1,3] Tae-Hwan Jang,[2]
Younghak Kim,[4] Jae-Young Kim,[3] Sang-Wook Cheong,[5,6] and Jae-Hoon Park[1,2,7,*]

[1]*Department of Physics, POSTECH, Pohang 37673, Korea*
[2]*MPPHC-CPM, Max Planck POSTECH/Korea Research Initiative, Pohang 37673, Korea*
[3]*Center for Artificial Low Dimensional Electronic Systems, IBS, Pohang 37673, Korea*
[4]*Pohang Accelerator Laboratory, POSTECH, Pohang 37673, Korea*
[5]*Laboratory for Pohang Emergent Materials and Max Plank POSTECH Center for Complex Phase Materials,
POSTECH, Pohang 37673, Korea*
[6]*Rutgers Center for Emergent Materials and Department of Physics and Astronomy, Rutgers University,
Piscataway, New Jersey 08854, USA*
[7]*Division of Advanced Materials Science, POSTECH, Pohang 37673, Korea*

We propose a novel origin of magnetic anisotropy to explain the unusual magnetic behaviors of layered ferromagnetic Cr compounds ($3d^3$) wherein the anisotropy field varies from $\lesssim 0.01$ to ~ 3 T on changing the ligand atom in a common hexagonal structure. The effect of the ligand p orbital spin-orbit (LS) coupling on the magnetic anisotropy is explored by using four-site full multiplet cluster model calculations for energies involving the superexchange interaction at different spin axes. Our calculation shows that the anisotropy energy, which is the energy difference for different spin axes, is strongly affected not only by the LS coupling strength but also by the degree of p-d covalency in the layered geometry. This anisotropy energy involving the superexchange appears to dominate the magnetic anisotropy and even explains the giant magnetic anisotropy as large as 3 T observed in CrI_3.

Quantum fluctuation becomes more effective in low-dimensional magnetic systems and often realizes exotic quantum ground states such as the spin-1 Haldane gap state in one dimension (1D) chain systems [1,2] and the spin liquid state with anyonic excitation in 2D layered Kitaev systems [3–5], differently from the ordinary ferromagnetic or antiferromagnetic ordered ground state. The Mermin-Wagner theorem even tells us that no long-range order can persist in the 2D Heisenberg magnetic system due to the strong spin fluctuation [6]. Meanwhile, the magnetically ordered ground state has been observable in several 2D-like layered systems and attributed to an imperfection of the two-dimensionality caused by nonvanishing interlayer coupling in real materials [7–11].

Recently, true 2D ferromagnetism has been realized in single-layer CrI_3 [12] and also in $Cr_2Ge_2Te_6$ pristine double layers [13]. Considering the Cr^{3+} (t_{2g}^3; $^4A_2$) ionic state with minimal orbital angular momentum ($L \simeq 0$), these discoveries are surprising, since the magnetocrystalline anisotropy ($\xi \boldsymbol{L} \cdot \boldsymbol{S}$) is sufficiently small for the system to be considered as a near-Heisenberg magnetic system. On the other hand, bulk CrI_3 has been observed to exhibit giant magnetic anisotropy energy. This strong anisotropy is speculated to suppress the spin fluctuation significantly to realize ferromagnetism even in a true 2D system [12,13]. However, the presence of giant magnetic anisotropy itself in Cr compounds with $L \simeq 0$ contradicts current explanations on the magnetic anisotropy, and its origin has been puzzling.

CrX_3 ($X = $ Cl, Br, and I) and $CrYTe_3$ ($Y = $ Ge and Si) are commonly crystallized in the $R\bar{3}$ rhombohedral structure [14–19]. Figure 1(a) shows the 2D atomic arrays of

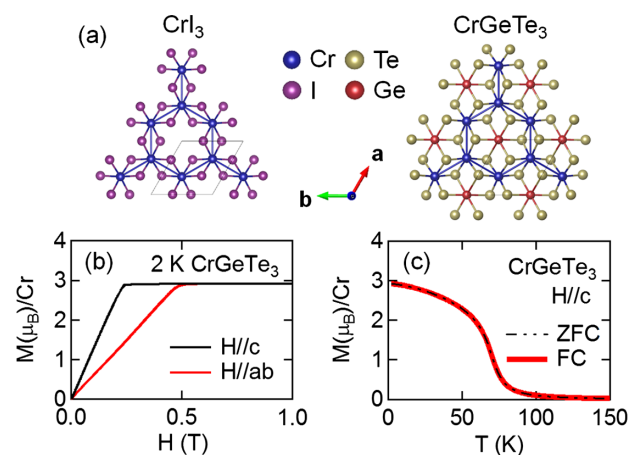FIG. 1. (a) Top views of CrI_3 (left) and $CrGeTe_3$ (right) layers. Cr, I, Ge, and Te are represented by blue, purple, red, and yellow spheres, respectively. (b) M-H curves corresponding to $H\|c$ and $H\|ab$ and (c) M-T curves measured on $CrGeTe_3$. Field cooling (FC) was processed under $H = 0.5$ T.

CrI_3 and $CrGeTe_3$ as representatives of both systems. Both structures are the so-called $1T$ AB_2 layered structure, in which one out of three A sites is empty (CrX_3) or replaced with a Ge or Si dimer ($CrYTe_3$). The trigonal distortion of CrX_6 octahedra is minimal in CrX_3, while the inserted dimer in $CrYTe_3$ considerably elongates the $CrTe_6$ octahedron along the trigonal (hexagonal) c axis.

These Cr compounds are all magnetic insulators with a local magnetic moment near $3\mu_B$/Cr, of which the intralayer interaction is ferromagnetic [14,19–24], as expected in the Goodenough-Kanamori rule for the 90° superexchange hopping path [25–27]. The interlayer coupling is ferromagnetic except in the case of $CrCl_3$, in which it is antiferromagnetic but sufficiently weak for the ordering to become ferromagnetic even under a small magnetic field (<0.01 T) [18,22]. Such a minimal interlayer interaction was also reported in inelastic neutron scattering and critical exponent analysis studies on other layered Cr compounds such as $CrBr_3$ and $CrYTe_3$ [28–31]. These layered ferromagnets, including $CrCl_3$, commonly exhibit a soft magnet behavior of a linear M-H curve before saturation with either zero or a minimal (<0.01 T) coercive field [18–22,29,32] and zero deviation in the field cooling in the M-T curve, as shown in Figs. 1(b) and 1(c) for $CrGeTe_3$ as an example, respectively. Similar magnet behaviors were also reported in other quasi-2D ferromagnets such as Fe_3GeTe_2 and K_2CuF_4 [33,34].

In addition to the soft magnet behaviors, we can also observe a large difference in the saturation magnetic field for $H\|c$ (H_c^S) and $H\|ab$ (H_{ab}^S), as shown in Fig. 1(b). Remarkably, the anisotropy field $\Delta H^S = H_c^S - H_{ab}^S$ varies from ≲0.01 T ($CrCl_3$) to ~3 T (CrI_3) on changing only the ligand environment (see Table S1 in Supplemental Material [35]). This large variation contradicts the general explanation with two leading terms of the single-ion (magnetocrystalline) and shape (dipole-dipole) magnetic anisotropies, which are too small to explain the variation. The single-ion anisotropy originates from anisotropy in L, mostly quenched in the Cr^{3+} t_{2g}^3 ($^4A_2$;^4S) compounds, with the energy $\Delta E_{LS} = -\xi\Delta LS/4$. The Cr $3d$ LS coupling energy $\xi\boldsymbol{L}\cdot\boldsymbol{S}$ partially admixes the t_{2g} and e_g orbitals to restore small values of $L \sim 2\xi/10$ Dq $\simeq 0.06$ for $\xi(Cr3d) \simeq 30$ meV and 10 Dq ~ 1 eV. Indeed, we obtained $L \sim 0.05$ and one or 2 orders of magnitude smaller ΔL values in both the Cr $L_{2,3}$-edge x-ray magnetic circular dichroism (XMCD) measurements and the theoretical cluster model calculations [35]. The resulting ΔE_{LS} is ~0.04 meV (~0.2 T) for $CrGeTe_3$ and ~0.004 meV (~0.02 T) for CrI_3. The shape anisotropy commonly favors the in-plane easy axis in the layered materials. The magnitude is roughly $\Delta E_{dipole} \simeq \mu_0 m^2/4\pi r^3 \sim 0.02$ meV (~0.1 T).

Figure 2 displays the magnetic anisotropy energy $\Delta E_K = 3\mu_B\Delta H^S$ at a low temperature as a function of the ligand p spin-orbit coupling strength ξ_p. Interestingly, $|\Delta H^S|$ greatly increases with an increase in ξ_p except
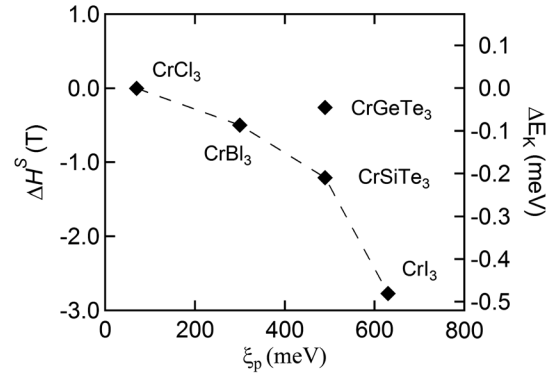

FIG. 2. Anisotropy fields ΔH^S and magnetic anisotropy energies ΔE_K of various layered Cr compounds, $CrCl_3$ [18,22], $CrBr_3$ [21], CrI_3 [19], $CrGeTe_3$ [29], and $CrSiTe_3$ [32], as a function of the ligand p spin-orbit coupling strength ξ_p.

for $CrGeTe_3$, thus implying that significant magnetic anisotropy is additionally contributed by the ligand p electrons. Indeed, a recent first principles band calculation study on CrI_3 suggested the role of I $5p$ spin-orbit coupling to explain the giant magnetic anisotropy [41]. One may suspect a possible contribution of the single-ion anisotropy via the ligand p state, which is also spin polarized through hybridization with the Cr $3d$ state. However, the ligand p single-ion anisotropy turns out to be negligible in the I $M_{4,5}$-edge (I $3d \rightarrow 5p$) XMCD study on CrI_3 with the largest ξ_p value of 0.63 eV (see Fig. S3 in Supplemental Material [35]).

Another possibility to consider could be a magnetic anisotropy term contributed by ξ_p through Cr $3d$-ligand p-Cr $3d$ superexchange hopping in the near 90° bonding angle networks. The large ξ_p splits the ligand p state into the total angular momentum $j_{3/2}$ and $j_{1/2}$ states. As an example, let us consider the Cr d_{yz}-ligand $p_{j_{1/2}}$-Cr $d_{3x^2-r^2}$ superexchange electron hopping channel for two different spin axes, $\boldsymbol{M}\|\hat{y}$ and $\boldsymbol{M}\|\hat{z}$, as depicted in Figs. 3(a) and 3(b), respectively. Here, $|j = 1/2, m_j = -1/2\rangle$ was chosen for the ligand $p_{j_{1/2}}$ on purpose (the hopping actually vanishes for $|1/2, +1/2\rangle$). This $j_{1/2}$ state is an admixed state in both spin and orbital states and is represented as $(p_{x,+\sigma_z} - ip_{y,+\sigma_z} - p_{z,-\sigma_z})/\sqrt{3}$ in the conventional $\hat{z}$-spin axis, i.e., $\boldsymbol{M}\|\hat{z}$. However, when the spin axis changes to the $\hat{y}$ axis, the $j_{1/2}$ state becomes $(p_{z,+\sigma_y} - ip_{x,+\sigma_y} - p_{y,-\sigma_y})/\sqrt{3}$. Here, $\pm\sigma_y$ and $\pm\sigma_z$ denote the up and down spin along the $\hat{y}$- and $\hat{z}$-spin axes, respectively.

The hopping channel is represented by consecutive electron hoppings of the ligand p to $3d$ in one Cr site through ligand $p(j_{1/2})$-Cr e_g ($d_{3x^2-r^2}$) hybridization and t_{2g} in the other Cr site to ligand p ($j_{1/2}$) through d_{yz}-$j_{1/2}$ hybridization. We note that the orbital-geometry symmetry allows only the p_x-$d_{3x^2-r^2}$ ($pd\sigma$) and d_{yz}-p_z ($pd\pi$) hybridizations. Considering that the hybridization is spin independent, d_{yz}-p_z hybridization vanishes for $\boldsymbol{M}\|\hat{z}$ due to their different spin states, $+\sigma_z$ and $-\sigma_z$, respectively. As a result,
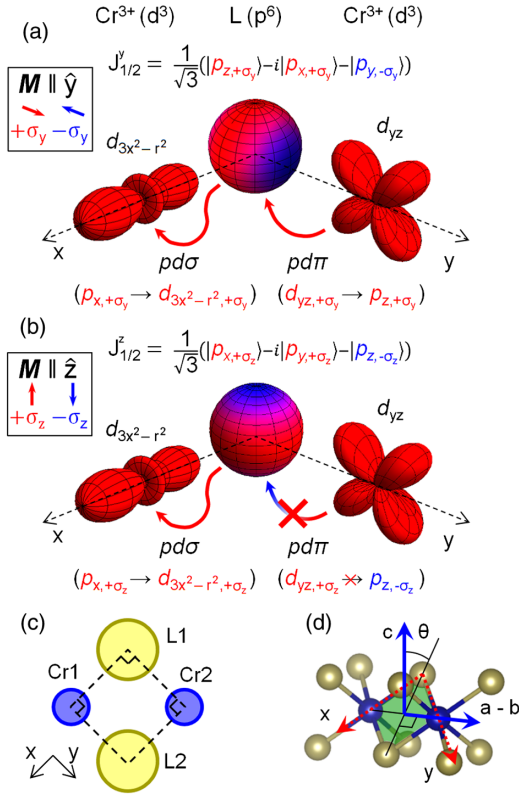
FIG. 3. Cr d_{yz}-L $p_{j_{1/2}}$-Cr $d_{3x^2-r^2}$ superexchange for (a) $\boldsymbol{M}\|\hat{y}$ and (b) $\boldsymbol{M}\|\hat{z}$. The spin states are indicated by red ($+\sigma_{y,z}$) and blue ($-\sigma_{y,z}$) colors. (c) Two equivalent 90° superexchange paths through ligands ($L1$ and $L2$) between two adjacent Cr atoms. (d) Cr-L-Cr local network (red dashed line) in the crystal coordinates (a and c).
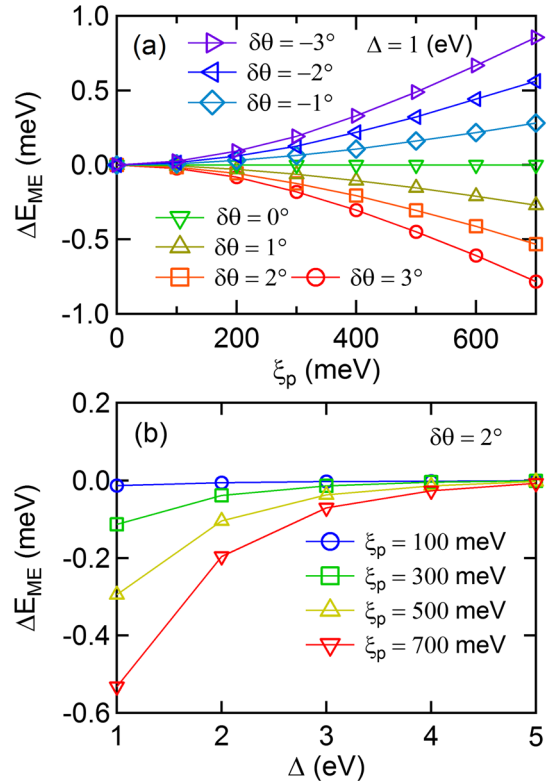

FIG. 4. Four-site full multiplet cluster model calculation results for ΔE_{ME} as functions of (a) ξ_p for various $\delta\theta$ values at $\Delta = 1$ eV and of (b) Δ for various ξ_p values at $\delta\theta = 2°$.

superexchange hopping is allowed only for the spin axis $\boldsymbol{M}\|\hat{y}$ though nonvanishing $p_{x,+\sigma_y}$-$d_{3x^2-r^2,+\sigma_y}$ and $d_{yz,+\sigma_y}-p_{z,+\sigma_y}$ hybridizations. Therefore, this superexchange hopping path contributes a magnetic anisotropy term favoring $\boldsymbol{M}\|\hat{y}$ (in plane). The magnetic anisotropy contribution varies with the hopping channel, and the net magnetic anisotropy, the so-called magnetic exchange anisotropy, can be determined by summing the contributions for all possible Cr t_{2g}, ligand p, Cr e_g orbital combination channels of the superexchange hopping.

In layered Cr compounds, two equivalent ligands exist between two neighboring Cr sites with a near 90° bonding angle. Thus, we performed full multiplet cluster calculations for a four-site ansatz in the edge-shared plane consisting of two Cr and two ligand sites [Fig. 3(c)] to quantify the magnetic exchange anisotropy. In the calculation, we took into account the full atomic multiplets as well as all configurations up to charge transferred three-hole states at the ligand sites (see Supplemental Material, Sec. III [35], for details). In the layered Cr compounds, the edge-shared (xy) plane has an off-angle θ from the crystal c axis as shown in Fig. 3(d). Angle θ in the crystal structure, which slightly deviates from $\theta_{O_h} \simeq 35.3°$ by the degree of

trigonal distortion, is utilized for the determination of the net magnetic exchange anisotropy $\Delta E_{\mathrm{ME}} = E_{\mathrm{ME}}^c - E_{\mathrm{ME}}^{ab}$, which vanishes at the deviation angle $\delta\theta = \theta_{O_h} - \theta = 0$.

Figure 4 displays the calculated ΔE_{ME} as a function of (a) ξ_p for different $\delta\theta$ values and of (b) ligand p to Cr $3d$ charge transfer energy Δ for different ξ_p values. Here, the number ($z = 3$) of equivalent neighboring Cr sites is taken into account. Parameter values such as the $3d$ on-site Coulomb energy U_{dd} and the hybridization strengths $pd\sigma/pd\pi$ are taken from the cluster model analyses of the Cr $L_{2,3}$-edge XAS/XMCD results of CrI$_3$ (see Table S2 in Supplemental Material [35]). Since ΔE_{ME} basically originates from the spin-axis-dependent superexchange hopping in the hexagonal structure, its magnitude is mainly determined by three factors: the degree of spin state mixing involving ξ_p, the superexchange energy scale varying with Δ, and the geometry factor in the exchange anisotropy in the hexagonal structure [see Fig. 3(d)] represented with $\delta\theta$ driven by the trigonal distortion, resulting in a power law form of $\Delta E_{\mathrm{ME}} \propto (\xi_p)^{\alpha}(\delta\theta)^{\beta}/(\Delta)^{\gamma}$. Indeed, the full calculation results turn out to be suitably represented by this form with $\alpha \simeq 1.7$, $\beta \simeq 1$, and $\gamma = 1.5$–1.9 (see Supplemental Material, Sec. IV [35]). For a given Δ value, ΔE_{ME} increases with ξ_p and reaches up to 0.9 meV for $\xi_p = 700$ meV and $\delta\theta = 3°$. This means that ΔE_{ME} is sufficiently large to explain the largest anisotropy energy

TABLE I.   Parameters used in model calculations and magnetic anisotropy energies obtained from calculations as described in the text. Here, $\delta E_K = \Delta E_{LS} + \Delta E_{\text{dipole}}$.

	$CrCl_3$	$CrBr_3$	CrI_3	$CrGeTe_3$	$CrSiTe_3$
ξ_p (meV)	70	300	630	490	490
$\delta\theta$ (°)	2	2	2	7	7
Δ (eV)	3.5	1.5	1.2	2.2	2.2
ΔE_{ME} (meV)	$\lesssim 0.001$	-0.084	-0.47	-0.27	-0.27
Δ' (eV)	None	None	None	1.3	2.0
$\Delta E'_{\text{ME}}$ (meV)	None	None	None	0.17	0.01
δE_K (meV)	0.01	0.01	0.01	0.06	0.06
ΔE_K^{th} (meV)	0.01	-0.074	-0.46	-0.040	-0.21
$\Delta E_K^{\exp}$ (meV)	$\lesssim 0.001$	-0.086	-0.48	-0.045	-0.21

$\Delta E_K \sim 0.5$ meV required for CrI_3 (see Fig. 2), which has $\xi_p = 630$ meV and $\delta\theta \simeq 2°$. Indeed, the observed magnetic anisotropy $\Delta E_K^{\exp}$ agrees closely with the estimated ΔE_{ME} with reasonable Δ for CrX_3 and $CrSiTe_3$ with different ligands after correction $\delta E_K = \Delta E_{LS} + \Delta E_{\text{dipole}}$ of the single-ion and shape anisotropy contributions estimated from the XMCD and numerical magnetic dipole energy analyses, as summarized in Table I. The correction is somewhat large in $CrYTe_3$ by its sizable ΔE_{LS} (~ 0.04 meV) resulting from the greatly elongated $CrTe_6$ octahedron due to the inserted A-site dimer.

Despite the fact that $CrGeTe_3$ has the same Te ligands as $CrSiTe_3$, its ΔE_K is reduced significantly from that of $CrSiTe_3$, thus indicating that the A-site dimer considerably affects the electronic structure of the Te $5p$ states. In fact, the Ge or Si dimer forms a strong covalent bond with Te to split the Te $5p$ band into the bonding (occupied) and antibonding (unoccupied) states. As a result, the ordinary Te $5p$ to Cr $3d$ charge transfer energy Δ effectively increases, and a new charge transfer from Cr $3d$ to the unoccupie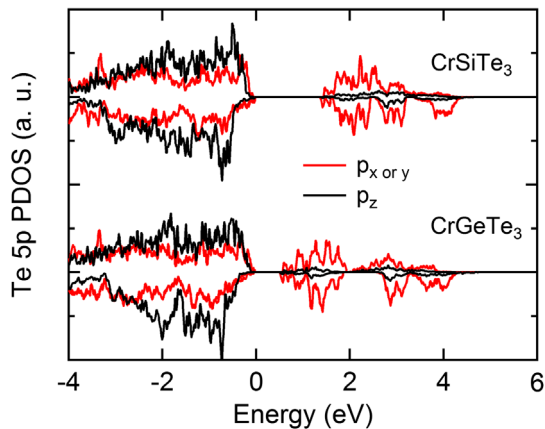d Te $5p$ is introduced. Figure 5 presents the density of states (DOS) of the Te $5p$ orbital states for $CrGeTe_3$ and $CrSiTe_3$ obtained from the wannierized band structure calculations in the absence of Cr $3d$-Te $5p$ hybridization [35], which is explicitly taken into account in the cluster model calculations. As can be seen in the figure, the occupied Te $5p$ states are nearly the same in energy for these compounds, while a significant energy difference appears for the unoccupied states. The Cr $3d$ to the unoccupied Te $5p$ charge transfer energy Δ' of $CrGeTe_3$ is estimated to be smaller by 0.7 eV than that of $CrSiTe_3$ through weighted averaging. This new charge transfer opens additional Cr $3d$-unoccupied Te $5p$-Cr $3d$ super-exchange channels and contributes an additional magnetic exchange anisotropy, which significantly reduces the magnetic anisotropy ΔE_K in $CrGeTe_3$ as can be inferred from Table I.

We have thus far demonstrated that the additional magnetic exchange anisotropy, induced by the ligand p spin-orbit coupling through the superexchange mechanism, suitably explains the large variation in the magnetic anisotropy energy of layered Cr compounds and is also responsible for the giant magnetic anisotropy observed in CrI_3 and $CrSiTe_3$. The magnetic exchange anisotropy introduces anisotropy in the spin-spin exchange interaction, thus resulting in an anisotropic Heisenberg spin Hamiltonian of the form

$$H = J_{xx}(S_x^1 S_x^2 + S_y^1 S_y^2) + J_{zz}S_z^1 S_z^2, \qquad (1)$$

which leads to the predicted realization of the ferromagnetic ground state in the 2D spin system [42], as observed in these compounds with $L \simeq 0$. Our results indicate that the magnetic exchange anisotropy can significantly contribute to the magnetic anisotropy for magnetic systems with large ligand spin-orbit coupling to realize true 2D ferromagnetism, and they also suggest a new approach to search giant magnetic anisotropy materials for potential applications to spintronic devices.

FIG. 5.   Partial density of state of Te $5p$ orbitals determined from wannierization on $CrGeTe_3$ and $CrSiTe_3$. Strong Si(Ge)-Te covalent bonding effectively pushes down the occupied bonding states by about 1.5 eV (weighted average) and transfers about 30% Te $5p$ weight to the unoccupied antibonding states.

*Corresponding author.
jhp@postech.ac.kr

[1] F. D. M. Haldane, Phys. Rev. Lett. 50, 1153 (1983).

[2] M. Kenzelmann, R. A. Cowley, W. J. L. Buyers, Z. Tun, R. Coldea, and M. Enderle, Phys. Rev. B **66**, 024407 (2002).

[3] A. Kitaev, Ann. Phys. (Amsterdam) **321**, 2 (2006).

[4] A. Banerjee, J. Yan, J. Knolle, C. A. Bridges, M. B. Stone, M. D. Lumsden, D. G. Mandrus, D. A. Tennant, R. Moessner, and S. E. Nagler, Science **356**, 1055 (2017).

[5] S.-H. Do, S.-Y. Park, J. Yoshitake, J. Nasu, Y. Motome, Y. Kwon, D. T. Adroja, D. J. Voneshen, K. Kim, T.-H. Jang, J.-H. Park, K.-Y. Choi, and S. Ji, Nat. Phys. **13**, 1079 (2017).

[6] N. D. Mermin and H. Wagner, Phys. Rev. Lett. **17**, 1133 (1966).

[7] X. Liu, T. Berlijn, W.-G. Yin, W. Ku, A. Tsvelik, Y.-J. Kim, H. Gretarsson, Y. Singh, P. Gegenwart, and J. P. Hill, Phys. Rev. B **83**, 220403(R) (2011).

[8] R. D. Johnson, S. C. Williams, A. A. Haghighirad, J. Singleton, V. Zapf, P. Manuel, I. I. Mazin, Y. Li, H. O. Jeschke, R. Valentí, and R. Coldea, Phys. Rev. B **92**, 235119 (2015).

[9] H. Ikeda and K. Hirakawa, J. Phys. Soc. Jpn. **35**, 722 (1973).

[10] K. M. Kojima, Y. Fudamoto, M. Larkin, G. M. Luke, J. Merrin, B. Nachumi, Y. J. Uemura, N. Motoyama, H. Eisaki, S. Uchida, K. Yamada, Y. Endoh, S. Hosoya, B. J. Sternlieb, and G. Shirane, Phys. Rev. Lett. **78**, 1787 (1997).

[11] H. Kadowaki, K. Ubukoshi, and K. Hirakawa, J. Phys. Soc. Jpn. **56**, 751 (1987).

[12] B. Huang, G. Clark, E. Navarro-Moratalla, D. R. Klein, R. Cheng, K. L. Seyler, D. Zhong, E. Schmidgall, M. A. McGuire, D. H. Cobden, W. Yao, D. Xiao, P. Jarillo-Herrero, and X. Xu, Nature (London) **546**, 270 (2017).

[13] C. Gong, L. Li, Z. Li, H. Ji, A. Stern, Y. Xia, T. Cao, W. Bao, C. Wang, Y. Wang, Z. Q. Qiu, R. J. Cava, S. G. Louie, J. Xia, and X. Zhang, Nature (London) **546**, 265 (2017).

[14] V. Carteaux, D. Brunet, G. Ouvrard, and G. Andre, J. Phys. Condens. Matter **7**, 69 (1995).

[15] R. E. Marsh, J. Solid State Chem. **77**, 190 (1988).

[16] L. L. Handy and N. W. Gregory, J. Am. Chem. Soc. **74**, 891 (1952).

[17] B. Morosin and A. Narath, J. Chem. Phys. **40**, 1958 (1964).

[18] A. A. McGuire, G. Clark, K. C. Santosh, W. M. Chance, G. E. Jellison, V. R. Cooper, X. Xu, and B. C. Sales, Phys. Rev. Mater. **1**, 014001 (2017).

[19] M. A. McGuire, H. Dixit, V. R. Cooper, and B. C. Sales, Chem. Mater. **27**, 612 (2015).

[20] H. Ji, R. A. Stokes, L. D. Alegria, E. C. Blomberg, M. A. Tanatar, A. Reijnders, L. M. Schoop, T. Liang, R. Prozorov, K. S. Burch, N. P. Ong, J. R. Petta, and R. J. Cava, J. Appl. Phys. **114**, 114907 (2013).

[21] J. J. F. Dillon, J. Phys. Soc. Jpn. **19**, 1662 (1964).

[22] A. Narath and H. L. Davis, Phys. Rev. **137**, A163 (1965).

[23] V. Carteaux, G. Ouvrard, J. Grenier, and Y. Laligant, J. Magn. Magn. Mater. **94**, 127 (1991).

[24] I. Tsubokawa, J. Phys. Soc. Jpn. **15**, 1664 (1960).

[25] J. B. Goodenough, Phys. Rev. **100**, 564 (1955).

[26] J. B. Goodenough, J. Phys. Chem. Solids **6**, 287 (1958).

[27] J. Kanamori, J. Phys. Chem. Solids **10**, 87 (1959).

[28] E. J. Samuelsen, R. Silberglitt, G. Shirane, and J. P. Remeika, Phys. Rev. B **3**, 157 (1971).

[29] G. T. Lin, H. L. Zhuang, X. Luo, B. J. Liu, F. C. Chen, J. Yan, Y. Sun, J. Zhou, W. J. Lu, P. Tong, Z. G. Sheng, Z. Qu, W. H. Song, X. B. Zhu, and Y. P. Sun, Phys. Rev. B **95**, 245212 (2017).

[30] T. J. Williams, A. A. Aczel, M. D. Lumsden, S. E. Nagler, M. B. Stone, J.-Q. Yan, and D. Mandrus, Phys. Rev. B **92**, 144404 (2015).

[31] B. Liu, Y. Zou, L. Zhang, S. Zhou, Z. Wang, W. Wang, Z. Qu, and Y. Zhang, Sci. Rep. **6**, 33873 (2016).

[32] L. D. Casto, A. J. Clune, M. O. Yokosuk, J. L. Musfeldt, T. J. Williams, H. L. Zhuang, M.-W. Lin, K. Xiao, R. G. Hennig, B. C. Sales, J.-Q. Yan, and D. Mandrus, APL Mater. **3**, 041515 (2015).

[33] K. Kim, J. Seo, E. Lee, K.-T. Ko, B. S. Kim, B. G. Jang, J. M. Ok, J. Lee, Y. J. Jo, W. Kang, J. H. Shim, C. Kim, H. W. Yeom, B. Il Min, B.-J. Yang, and J. S. Kim, Nat. Mater. **17**, 794 (2018).

[34] S. Hirata, N. Kurita, M. Yamada, and H. Tanaka, Phys. Rev. B **95**, 174406 (2017).

[35] See Supplemental Material at http://link.aps.org/supplemental/10.1103/PhysRevLett.122.207201 for the details about the estimation of magnetic anisotropy energies, which includes Refs. [36,37], and the technical details about the wannierized band structure calculations, which includes Refs. [38–40].

[36] A. Tanaka and T. Jo, J. Phys. Soc. Jpn. **63**, 2788 (1994).

[37] C. T. Chen, Y. U. Idzerda, H.-J. Lin, N. V. Smith, G. Meigs, E. Chaban, G. H. Ho, E. Pellegrin, and F. Sette, Phys. Rev. Lett. **75**, 152 (1995).

[38] I. Souza, N. Marzari, and D. Vanderbilt, Phys. Rev. B **65**, 035109 (2001).

[39] P. Giannozzi et al., J. Phys. Condens. Matter **21**, 395502 (2009).

[40] R. Sakuma, Phys. Rev. B **87**, 235109 (2013).

[41] J. L. Lado and J. Fernández-Rossier, 2D Mater. **4**, 035002 (2017).

[42] E. E. Reinehr and W. Figueiredo, Phys. Rev. B **52**, 310 (1995).